

Nuclear spin relaxation in aqueous paramagnetic ion solutions

David A. Faux,¹ Örs Istók,¹ Arifah A. Rahaman,¹ Peter J. McDonald,¹ Eoin McKiernan,²
and Dermot F. Brougham²

¹*Department of Physics, University of Surrey, Guildford, GU2 7XH, UK.*^{a)}

²*School of Chemistry, University College Dublin, Belfield, Dublin 4, Ireland.*

(Dated: 14 September 2021)

An angular time-dependent probability density function describing Brownian or anomalous rotational dynamics of fixed-length atom-to-atom vectors is presented. The probability density function, which fully incorporates angular boundary conditions, is applied to aqueous ion complexes. The rotational dynamics of ion-¹H vectors are shown by molecular dynamics (MD) simulation to be Brownian. A Brownian shell model is presented which yields a closed form expression for the frequency-dependent nuclear-magnetic-resonance spin-lattice relaxation rate $T_1^{-1}(\omega)$ based on a distance parameter and time constant. Appropriate combinations of shell and/or continuum models are shown to provide excellent fully-quantitative fits to experimental $T_1^{-1}(\omega)$ dispersion curves from aqueous manganese(II), iron(III) and copper(II) chloride solutions. The distance parameters and time constants obtained from the fits are in good agreement with independent experimental and MD data in the literature. The Brownian shell model is a significant enhancement to existing particle-particle models that describe the rotational correlation function as a single exponential and are unable to provide the correct distance dependence for a shell of ¹H spin density preventing a match to experiment without an arbitrary scaling factor.

Keywords: nuclear spin relaxation, rotational dynamics, aqueous ions

^{a)}Electronic mail: d.faux@surrey.ac.uk

I. INTRODUCTION

Paramagnetic ions possess unpaired electrons which give rise to a spin with a large magnetic moment. The electron magnetic moment is more than 600 times stronger than that due to the proton with the result that the nuclear magnetic resonance (NMR) properties of solutions containing paramagnetic ions are dominated by the interaction of the nuclear spins of the solvent protons with the electronic spin of the paramagnetic ions.

Nuclear magnetic resonance was first used to study nuclear spin relaxation in aqueous paramagnetic ion solutions in 1948 by Bloembergen, Purcell and Pound¹. This seminal work measured the spin-lattice (longitudinal) relaxation time T_1 for aqueous solutions containing Mn^{2+} , Fe^{3+} , and Cu^{2+} ions. More than 70 years later, high-performance fast-field-cycling NMR (FFC-NMR) spectrometry yields $T_1^{-1}(\omega)$ typically across a frequency range $f = \omega/2\pi$ from 0.01 MHz to 20 MHz. The dispersion curves are exquisitely sensitive to the relative motion of pairs of spins over timescales from picoseconds to microseconds and FFC-NMR is therefore applied to a vast and increasing range of fluids and fluid-bearing materials containing paramagnetic ions. For instance, manganese may be used as a contrast agent^{2,3} for many applications but especially in biochemistry and medicine⁴, $T_1^{-1}(\omega)$ dispersion curves obtained from liquids in the food industry^{5,6} can be used to identify the paramagnetic ion type, and aqueous paramagnetic ions contribute to the relaxation rates measured from a broad range of fluid-bearing porous materials including cementitious materials, catalysts, silica material, glasses, zeolites and clays, to name but a few⁷.

The longitudinal relaxation rate $T_1^{-1}(\omega)$ at Larmor frequency ω for paramagnetic ions in aqueous solution is dominated by the dipolar interaction of the nuclear 1H spin of water (I) with the electronic spin (S) of the aqueous paramagnetic ion. Relaxation arises due to the relative motion of pairs of spins. The water surrounding a paramagnetic ion is typically categorised to one of two environments. The inner-sphere water (first coordination shell) is the water in contact with the ion. The second environment is the outer-sphere water which is considered here to comprise all water not in the inner sphere. Water exchanges between the two environments. Each dynamical process occurs at a different timescale resulting in highly-complex $S-I$ relative spin dynamics.

Nuclear magnetic resonance relaxometry measurements of $T_1^{-1}(\omega)$ yield a dispersion curve that captures information on the relative motion of $S-I$ spin pairs over timescales span-

ning many orders of magnitude. Solomon, Bloembergen, Morgan and others⁸⁻¹² adopted a simplified model of the relative spin dynamics, later called the SBM model, leading to a simple expression for $T_1^{-1}(\omega)$ producing a good match to inflection features of experimental dispersion curves. The $S-I$ interaction is a strong function of distance and the SBM model identifies the key contributor to the relaxation rate dispersion as the dipolar interaction between the ion and the ^1H spins in the inner sphere. The SBM model is an example of a “shell model” which places all ^1H spins at a fixed distance from the ion. The angular rotation of the shell can then be described by a single exponentially-decaying function that translates into a neat analytic expression for the relaxation rate. The SBM model has since been the first port of call for the interpretation of relaxation rate dispersion curves from liquids that contain paramagnetic ions. The excellent book by Bertini, Luchinat and Parigi¹³ illustrates the application of the SBM to a range of aquoions.

In this article, we look afresh at the description of the dipolar interaction between a paramagnetic ion and the water ^1H spins that surround it. This work is motivated by the publication of a generalised description of the anomalous (Lévy) rotational diffusion of fixed-length atom-to-atom vectors that fully accounts for angular boundary conditions¹⁴. The model is applied to ion- ^1H fixed-length vectors in section II and validated by molecular dynamics (MD) simulation in section III confirming that, for aquoions, Brownian rotational dynamics is a good approximation. The simplification to Brownian dynamics leads to a closed form expression for the NMR spectral density functions presented in section II B 1.

Fast-field cycling NMR experiments are undertaken on aqueous solutions of manganese(II), iron(III) and copper(II) chloride at room temperature at a range of concentrations. We show that appropriate combinations of the Brownian shell models and continuum models provide excellent fits to FFC-NMR dispersion curves from aqueous solutions of paramagnetic ions across the full frequency range. The numerical values of the fit parameters provide insight into the dynamic processes that contribute to the relaxation rate response and provide a clearer explanation for the position and number of inflection features appearing in the dispersion curve. It is demonstrated that dipolar $S-I$ interactions alone satisfactorily describe the dispersion curve for these aquoions.

The outline theory for the Brownian shell model and alternative models are presented in section II with more detail presented in the appendix. The underpinning assumptions are tested and validated through MD simulations described in section III. The experimentation

is detailed in section IV and the model is fit to the NMR dispersion curves using various inner-outer-sphere model combinations in section V. Finally, the key results are summarised in section VI.

II. THEORY

A. General background

The spin-lattice (longitudinal) relaxation rate $T_1^{-1}(\omega) = R_1(\omega)$ arises due to fluctuations in the dipolar interaction between the electronic spin (S) of a paramagnetic ion and a nuclear spin (I) of a water proton. On the assumption that the electronic spin is located at the center of the paramagnetic ion, and within the fast-diffusion approximation¹⁵, the relaxation rate may be written^{16,17}

$$T_1^{-1}(\omega) = R_1(\omega) = \frac{1}{3}\beta_{IS} [7J(\omega_S) + 3J(\omega)] \quad (1)$$

where $\beta_{IS} = (\mu_0/4\pi)^2 \gamma_I^2 \gamma_S^2 \hbar^2 S(S+1)$, and γ_S (γ_I) is the gyromagnetic ratio for the electronic (nuclear) spin. The Larmor angular frequency of the electronic spin in the applied static field is $\omega_S = 658.21\omega$ and $\omega = 2\pi f$. The spectral density functions $J(\omega)$ are obtained from the Fourier transformation of the dipolar correlation function $G(t)$ using the expression

$$J(\omega) = 2 \int_0^\infty G(t) \cos \omega t dt. \quad (2)$$

The key to developing a model describing the frequency-dependence of NMR relaxation rates is the determination of the dipolar correlation function $G(t)$. $G(t)$ captures all the relevant dynamical information describing how pairs of spins move relative to each other. In three-dimensional (3D) systems, such as unconfined fluids, $G(t)$ may be determined using the expression^{18,19}

$$G(t) = \left\langle \frac{P_2(\cos \beta)}{r_0^3 r^3} \right\rangle \quad (3)$$

where r_0 and r are the magnitudes of vectors connecting the center of a paramagnetic ion to a proton spin at time $t=0$ and the same spin pair at time t respectively. The angle between the vectors \mathbf{r} and \mathbf{r}_0 is β as illustrated in Fig.1. The function $P_2(x) = \frac{1}{2}(3\cos^2 x - 1)$ is a Legendre polynomial. The angular bracket of Eq. (3) indicates the average over an ensemble of spin pairs.

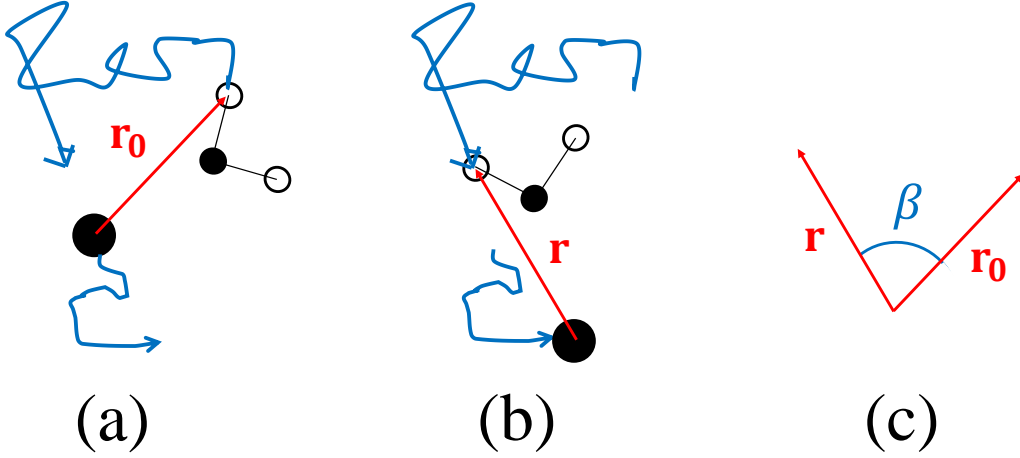


FIG. 1: In (a), at $t = 0$, a vector \mathbf{r}_0 extends from the paramagnetic ion to a hydrogen atom of a water molecule. In (b), time t later, both the ion and the water molecule have moved and \mathbf{r} links the ion to the same hydrogen atom. (c) shows the angle β between the two spin-pair vectors.

The water in aqueous ion systems can be identified with one of two environments: water in the inner sphere of the ion, and the water in the outer sphere. The motion of the inner-sphere water is restricted by its interaction with the ion whereas the outer-sphere water has dynamical characteristics similar to that of bulk water. Water exchanges between the inner and outer spheres. A description of key terms used in this article is presented in table I.

The dipolar correlation function $G(t)$ is required for the $S-I$ interactions for ^1H spins in each environment. A fraction x of all ^1H spins occupies the inner sphere and the remaining fraction $1-x$ occupies the outer sphere. The spin-lattice relaxation rates associated with the inner and outer spheres are R_{1i} and R_{1o} respectively. Provided that the rate of exchange of ^1H spins between the two environments is faster than the experimental relaxation rate $R_1(\omega)$, $R_1(\omega)$ is the average of the relaxation rate for the inner and outer spheres weighted by the fraction of spins in each environment²⁰, thus

$$R_1 = xR_{1i} + (1-x)R_{1o}. \quad (4)$$

The possible choices of model to describe the inner- and outer-sphere contributions to a measured spin-lattice relaxation rate are surveyed in the following section. The objective is to identify a combination of inner- and outer-sphere models that captures the dynamics of

TERM	DESCRIPTION
Inner sphere	The inner sphere refers to water contained in the first hydration shell of the ion (often referred to as the first coordination sphere). The inner sphere often contains about six water molecules.
Outer sphere	The outer sphere refers to all water not contained in the inner sphere of the ion.
Shell model	In a shell model, a volume of water ^1H spins are assumed to lie on a representative spherical shell of fixed radius with the ion at the center. The spin pair vector connecting the ion and a ^1H spin in the shell can change angle, but not length.
Inner shell model	The inner shell model places all the ^1H spins of the inner sphere water at a fixed distance a from the ion as illustrated in Fig. 2(a).
Outer shell model	The outer shell model places all ^1H spins of the outer sphere water at an effective distance d as illustrated in Fig. 2(b). <i>All</i> ^1H spins not in the inner sphere are included which is justified from a ^1H perspective by recognising that the dipolar $S-I$ interaction scales as r^{-4} .
Continuum model	A continuum model allows a uniform density of ^1H spins to occupy a region of space. The spin pair vector connecting the ion and a ^1H spin is assumed to change in length, but not angle. The continuum model presented by Abragam in 1961 ¹⁶ is illustrated in Fig. 2(c).
Hwang-Freed model	The Hwang–Freed continuum model ²¹ imposes a boundary condition that prevents particles moving closer together than d_{HF} as illustrated in Fig. 2(d). This model provides an improved physical description of the diffusion process and the considerable advantage of an analytical expression for the NMR spectral density functions.

TABLE I: Water surrounding an ion is associated with either the inner or outer sphere and described by a shell and/or continuum model. Important terms and their descriptions are presented.

$S-I$ spin pairs in each environment yielding expressions for $R_1(\omega)$ that are straightforward to compute, and which provide good fits to experimental FFC-NMR data obtained for a range of aqueous paramagnetic ions over the full frequency range of the experiment.

B. NMR models for aqueous paramagnetic ions

The measured NMR relaxation rate $R_1(\omega)$ is presumed to be due to the dipolar interaction of the electronic spin at the center of the paramagnetic ion with ^1H spins in both its inner and outer spheres. The $R_1(\omega)$ dispersion curve for aqueous Mn^{2+} , for instance, shows two inflection features each associated with a different characteristic time constant. The low-

frequency feature is indicative of slow motions and is associated with the rotation of the inner sphere of ^1H spins in the magnetic field. The higher-frequency contribution is due to the relaxation of fast-moving water and is therefore associated with the ^1H spins in the outer sphere.

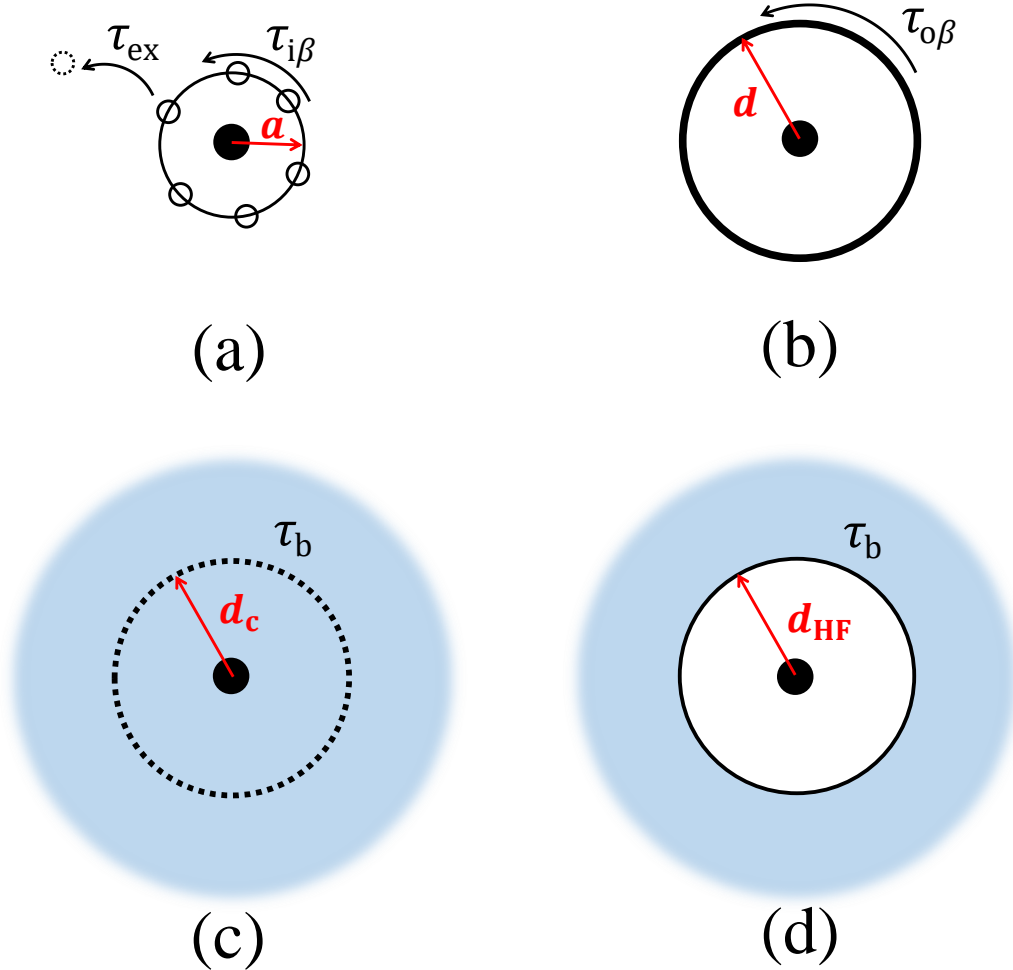


FIG. 2: The figure presents four inner or outer sphere models. Model (a) represents the inner shell model and shows a paramagnetic ion (\bullet) surrounded by six representative ^1H spins (\circ) constrained to a shell of radius a . The rotational time constant is $\tau_{i\beta}$ and τ_{ex} represents the inner-outer sphere water exchange lifetime. Model (b) is the outer shell model with all outer-sphere ^1H spins placed at a fixed distance d . The rotation of the shell is characterised by $\tau_{o\beta}$ (see text). Model (c) is a continuum model with a uniform ^1H spin density allowing water to diffuse through the inner-sphere space. Characterising parameters are a distance d_c and the bulk diffusion time constant τ_b . Model (d) represents the Hwang-Freed²¹ continuum model with a reflective boundary condition at $r = d_{\text{HF}}$.

Models are sought for time-dependent dipolar correlation functions, for the inner- and outer-spheres, $G_i(t)$ and $G_o(t)$ respectively, which capture the dynamics of the ^1H spins in the vicinity of a paramagnetic ion. These functions must be Fourier transformed using Eq. (2)

to yield $R_1(\omega)$ via Eqs. (1) and fit to experiment. The four candidate inner- and outer-sphere models presented in Fig. 2 reflect the most accessible and most common literature models for systems operating within the fast-diffusion limit. Terminology and time constants associated with the models discussed below are summarised in tables I and II.

TIME	DESCRIPTION
τ_i	A time constant that captures all dynamical processes associated with the inner sphere, for example through Eq. (6).
τ_{ex}	The exchange lifetime of a water molecule between the inner and outer sphere. If there are N_0 spins in the inner sphere at $t=0$, $N_0 \exp(-t/\tau_{\text{ex}})$ of those remain at time t later.
$\tau_{i\beta}$	Used in shell models, this is the rotational time constant associated with the inner shell. The time $2\tau_{i\beta}$ is the representative time for the ion complex comprising the inner-sphere water to rotate through one radian. $\tau_{i\beta}$ is typically of order microseconds.
$\tau_{o\beta}$	Used in shell models, this is the rotational time constant for the outer shell. The time $2\tau_{o\beta}$ is the representative time for the outer shell to rotate through one radian. In the context of H relaxation, it reflects the r^{-4} weighted average time for all the second coordination sphere ion- ^1H rotors to move through one radian. $\tau_{o\beta}$ is typically 25–40 ps.
τ_b	The translation diffusion time constant of the bulk water is defined in terms of the 3D self-diffusion coefficient D as $\tau_b = \delta^2/6D$. δ is set to 0.27 nm, the distance between one water oxygen and its nearest neighbor, so that a water molecule takes time τ_b to move a distance 0.27 nm in 3D. $\tau_b \approx 5.5$ ps for pure water at room temperature ²² .
τ_r	The rotational time constant used for the SBM model.
τ_e	The electronic spin relaxation time constant.

TABLE II: The dynamical time constants relevant to the SBM, shell and continuum models are presented and described.

In the following section the Solomon, Bloembergen and Morgan^{8–12} (SBM) model is presented. The dipolar correlation function $G_1(t)$ for both Brownian and anomalous (Lévy) shell models are then described followed by a summary of two continuum models.

1. Inner-sphere models

(i) The SBM particle–particle model

The Solomon, Bloembergen and Morgan^{8–12} SBM model is a particle–particle model

which can be applied to both the inner- and outer-sphere water. The SBM model applied to the inner sphere considers the decorrelation of the vector connecting the electronic point dipole at the ion center to an inner sphere ^1H spin. The assumption of Brownian rotational motion (and ignoring angular boundary conditions) leads to a dipolar correlation function $G_i(t) \propto \exp(-t/\tau_i)$ where τ_i is the relaxation timescale. The spectral density function may be expressed as

$$J(\omega) = \frac{A}{a^6} \left(\frac{2\tau_i}{1 + \omega^2\tau_i^2} \right) \quad (5)$$

where A is a constant proportional to the volume density of paramagnetic impurities. The term a^{-6} in the denominator of Eq. (5) signals a particle-particle model. The distance a is normally considered the distance of nearest approach of ^1H spins.

According to the SBM model, the time constant τ_i may be identified with several processes via²³

$$\frac{1}{\tau_i} = \frac{1}{\tau_r} + \frac{1}{\tau_{\text{ex}}} + \frac{1}{\tau_e} \quad (6)$$

where τ_r is a spin-pair-vector rotational time constant, the exchange time constant τ_{ex} is the characteristic residency time of the water molecule in the inner sphere (equivalently the time constant of the exponential time decay of inner-sphere water to the outer sphere), and τ_e is an electronic spin relaxation time constant. The frequency dependence of τ_e is sensitive to the paramagnetic ion and is discussed for the ions considered in this article in section II B 1(ii).

The SBM model assumes $G_i(t) \propto \exp(-t/\tau_i)$ whereby the exchange time τ_{ex} appears as $\exp(-t/\tau_{\text{ex}})$. Therefore, if there are N_0 spins in the inner sphere at $t = 0$, there are $N_0 \exp(-t/\tau_{\text{ex}})$ spins remaining at a time t later. Departing spins move into the outer sphere and are rapidly transported away. Equation (5) may be substituted into Eq. (1) to obtain a frequency-dependent relaxation rate that provides a good fit to many inflection features of FFC-NMR dispersion curves obtained from aqueous paramagnetic systems indicating that the important dynamical processes are captured by the SBM model. Its simplicity is attractive and the SBM model is often used to separately fit to both the inner and outer-sphere contributions in systems where there are two separate inflection features at different Larmor frequencies.

The SBM model is valid when dipolar interactions dominate and in the Redfield limit¹⁵ whereby the proton spins have explored all dynamical and physical environments during time

T_1 . The shortcomings of the SBM model are well known (see discussion by Kowalewski²⁴). In particular, the description of the rotational correlation function describing the $S-I$ pair vector as a single exponential function is limited and the model does not provide the correct distance dependence for a shell of ^1H spin density preventing a quantitative match to experiment without an arbitrary scaling factor. Due to more recent FFC-NMR data, it is now timely to revisit the problem and to provide an enhanced model that can produce a fully-quantitative fit to FFC-NMR nuclear spin relaxation dispersion curves obtained from aqueous paramagnetic ion solutions.

In the following section, a fully-developed theoretical description of Brownian rotational motion is presented which correctly presents the dipolar correlation function as a sum of exponentials, allows for fully quantitative fits to experimental data, and yet retains simplicity of implementation.

(ii) The Brownian inner shell model

The Brownian inner shell model assumes that the relaxation rate arises due to fluctuations of the spin-pair vector \mathbf{r} connecting the electronic spin of the paramagnetic ion to the ^1H spins of the water molecules set at a fixed distance $|\mathbf{r}_0|=|\mathbf{r}|=a$ as illustrated in Fig. 2(a). The dipolar correlation function for the inner shell, $G_i(t)$, is determined from the time-dependent probability density function $P(\beta, t)$ which is a function of the angle β between \mathbf{r} and \mathbf{r}_0 .

The probability density function $P(\beta, t)$ for a Brownian rotor is derived in the appendix through simplification of the analysis of a Lévy rotor. The Lévy rotor was introduced by Faux and co-workers¹⁴ as a model of anomalous rotational diffusion of the intra-molecular rotation of the $^1\text{H}-^1\text{H}$ vector in water. Lévy statistics is applied to systems where extreme angular changes occur more often than described by a Brownian model. The extent to which the rotational diffusion of β departs from Brownian motion is captured by the Lévy parameter α . Brownian rotational diffusion corresponds to $\alpha = 2$ and Lévy behavior is signalled by $\alpha < 2$. The rotational dynamics of the $S-I$ vector for aqueous ionic systems is investigated by MD simulation in section V A. It is found that $\alpha \approx 2$ and so Brownian dynamics is a satisfactory description in this case.

Setting $\alpha=2$ for the Brownian rotor allows the expansion of Eq. (A10) as an exponential series and the significant benefit of a final closed-form expression for the relaxation rate

dispersion. The series expansion with $\alpha=2$ yields,

$$G_i(t) = \frac{32\pi\delta N_M}{15a^4} \left[e^{-t/\tau_{i\beta}} + \frac{2}{3}e^{-2t/\tau_{i\beta}} + \left(\frac{2}{3}\right)^2 e^{-3t/\tau_{i\beta}} \dots \right] \quad (7)$$

where N_M is the number of paramagnetic ions per unit volume, $\delta = 0.27$ is a standard nanoscale distance. The rotational inner-shell time constant $\tau_{i\beta}$ in Eq.(7) is equivalent to $\tau/4$ in the appendix so that $2\tau_{i\beta}$ is the time taken for a rotation through one radian. The boundary conditions $0 \leq \beta \leq \pi$ provide the source of the exponential series expression of Eq.(7). The dipolar correlation function $G(t)$ is proportional to a^{-4} rather than a^{-6} for particle-particle models. The difference arises due to the averaging of the spin-spin interaction over the shell area.

It is straightforward to show that the third and subsequent terms of the expansion make a negligible contribution to $G_i(t)$. We therefore retain the first two terms of the expansion and multiply by a factor $\exp(-t/\tau_{\text{ex}})$ to account for the exchange of water molecules between the inner and outer coordination shells to obtain

$$G_i(t) = \frac{32\pi\delta N_M}{15a^4} \left[e^{-t/\tau_{i1}} + \frac{2}{3}e^{-t/\tau_{i2}} \right] \quad (8)$$

where

$$\frac{1}{\tau_{i1}} = \frac{1}{\tau_{i\beta}} + \frac{1}{\tau_{\text{ex}}} \quad \frac{1}{\tau_{i2}} = \frac{2}{\tau_{i\beta}} + \frac{1}{\tau_{\text{ex}}}. \quad (9)$$

The paramagnetic electronic spin relaxation time τ_e , which is included in Eq.(6), is omitted from Eq.(9). Bloembergen and co-workers^{1,12} discussed electronic spin relaxation in detail and Bertini *et al*¹³ summarise the likely contributions to relaxation rate dispersions for many important aquoions. Electronic spin relaxation can add a frequency-independent contribution to the dispersion. This is the case for Cu^{2+} ions. In the present work, any frequency-independent relaxation contributions are captured in a constant offset required to normalise experimental dispersion curves for a range of ion concentration to a single 1 mM master curve. Electronic spin relaxation can also add a frequency-dependent contribution. The electronic spin relaxation time constant τ_e for aqueous manganese(II) and iron(III) systems is usually in the range 10 ps–1 ns¹³. These timescales only influence the dispersion curve at the highest frequencies studied by FFC-NMR coinciding with the contribution of the outer-sphere water. An electronic spin relaxation contribution is clearly identifiable in the experimental relaxation rate dispersion for iron(III) at the highest frequency presented

later. It is demonstrated in section V that appropriate dipolar model combinations yield physically-reasonable fit parameters without scaling when fit to aqueous manganese(II), iron(III) and copper(II) systems, suggesting that the dipolar $S-I$ interaction dominates the dispersion for the three aquoion systems studied. Nonetheless, we cannot exclude the possibility that an unidentified electronic-spin contribution exists which contributes to the dispersion.

The Fourier transformation of $G_i(t)$ yields the spectral density function

$$J_i(\omega) = \frac{64\pi\delta N_M}{15a^4} \left[\frac{\tau_{i1}}{1+\omega^2\tau_{i1}^2} + \frac{\frac{2}{3}\tau_{i2}}{1+\omega^2\tau_{i2}^2} \right]. \quad (10)$$

Equation (10) is the spectral density function for the Brownian angular rotation of fixed-length spin-pair vectors with the time constant given by Eqs. (9). The inner-shell time constants τ_{i1} and τ_{i2} are dominated by the shorter of $\tau_{i\beta}$ or τ_{ex} and so it is useful to generate reduced forms of Eqn. (10) in the limits $\tau_{i\beta} \gg \tau_{\text{ex}}$ and $\tau_{i\beta} \ll \tau_{\text{ex}}$. These are

$$J_{i\beta}(\omega) = \frac{64\pi\delta N_M\tau_{i\beta}}{45a^4} \left[\frac{3}{1+\omega^2\tau_{i\beta}^2} + \frac{4}{4+\omega^2\tau_{i\beta}^2} \right] \quad \text{if } \tau_{i\beta} \ll \tau_{\text{ex}} \quad (11)$$

$$J_{\text{ex}}(\omega) = \frac{64\pi\delta N_M\tau_{\text{ex}}}{9a^4} \left[\frac{1}{1+\omega^2\tau_{\text{ex}}^2} \right] \quad \text{if } \tau_{i\beta} \gg \tau_{\text{ex}}. \quad (12)$$

The spectral density functions given by Eq (10) and simplifications given by Eqs. (11) and (12) may be substituted into Eq. (1) to obtain the frequency-dependent relaxation rate contribution for the Brownian inner shell model with parameters a , $\tau_{i\beta}$ and/or τ_{ex} .

2. *Outer-sphere models*

Three alternative models for relaxation associated with the outer sphere water are illustrated in Fig. 2 labelled as (b) for the Brownian outer-shell model, (c) for the continuous-diffusion model and (d) for the Hwang-Freed continuous-diffusion model.

The outer sphere refers to all water not in the inner sphere which, for 1 mM equivalent ion concentration corresponds to about 55,000 water molecules per cation. The water molecules are diffusing through the sample with a time constant τ_b , and relaxation arises due to changes in the length and orientation of vectors connecting an ion to the ^1H spins on the water molecules. The shell model illustrated in Fig. 2(b) simplifies the complex relative spin dynamics by placing all outer-sphere ^1H spins in a shell at a fixed distance d from

the ion. The distance d represents an average, or effective, distance recognising the r^{-4} dependence of the ion- ^1H spin dipolar interaction which defines a spherical surface within which relaxation is effective. The shell model allows relaxation due to the change in angle of the ion- ^1H spin vector (through the rotation of the shell) but ignores changes in vector length. By contrast, the continuum models illustrated in Fig. 2(c) and (d) accommodate changes in vector length but not angle.

(i) The Brownian outer shell model

The shell model introduced in section II may also be used as a model for the outer-sphere water as illustrated in Fig. 2(b). The spectral density function $J_{o\beta}(\omega)$ can be adapted from the inner-shell expression given by Eq. (11) to obtain

$$J_{o\beta}(\omega) = \frac{64\pi\delta N_M \tau_{o\beta}}{45d^4} \left[\frac{3}{1+\omega^2\tau_{o\beta}^2} + \frac{4}{4+\omega^2\tau_{o\beta}^2} \right] \quad (13)$$

where the rotational time constant for $S-I$ spin-pair vectors connecting to outer shell ^1H spins is $\tau_{o\beta}$. Equation (13) for the outer shell is taken directly from Eq. (11) for the inner shell. The outer shell rotational time constant is typically 20–35 ps so that even the shortest τ_{ex} satisfies $\tau_{\text{ex}} \gg \tau_{o\beta}^{25}$, and exchange of spins from the outer shell to the inner shell can be safely neglected.

(ii) The continuous-diffusion model

The continuous diffusion model has been widely used to describe intermolecular relaxation in liquids. The word “continuous” reflects the assumption that spins can diffuse unhindered through 3D space, and can therefore diffuse through each other. The dipolar correlation function may be expressed in a number of ways^{16,17,21,26,27} depending on the application. A suitable expression is¹⁷

$$G_o^{(c)}(t) = \frac{4\pi N_M}{d_c^3} \int_0^\infty \kappa^{-1} e^{-\delta^2\kappa^2 t/3d_c^2\tau_b} J_{3/2}^2(\kappa) d\kappa \quad (14)$$

where $J_{3/2}(x)$ is a half-integer Bessel function and κ is a Fourier variable. The water self-diffusion coefficient is defined as $D = \delta^2/6\tau_b$ where the standard nanoscale distance δ is equal to 0.27 nm and τ_b is a bulk diffusion time constant. The superscript “(c)” and subscript “c” refer to continuous diffusion. The distance d_c purports to be the distance of nearest approach of pairs of spins but is actually introduced as the lower limit of an integral to

avoid a numerical singularity that would arise if two spins were allowed to occupy the same position in space. The dependence of d_c^{-3} arises from a volume integral leading to Eq. (14).

Equation (14) is associated with Torrey²⁶ and Abragam¹⁶ who described the relative motion of pairs of nuclear spins in a liquid. Equation (14) has been widely used^{17,21,28,29} not least as a correction term that accounts for the contribution to the dipolar relaxation rate associated with the relative translational diffusion of pairs of spins that cannot be accounted for by a numerical simulation^{27,30}.

The dipolar correlation function given by Eq. (14) has to be computed numerically as a function of t for the chosen values of the parameters d_c and τ_b . The spectral density function $J_o^{(c)}(\omega)$ is then obtained by numerical Fourier transformation at each experimental frequency.

(iii) The Hwang-Freed model

The Hwang-Freed model²¹ is identical to the continuum diffusion model except that a boundary condition is introduced to prohibit spins from diffusing into a sphere of radius d_{HF} centered on the paramagnetic ion²¹. The result is an analytic expression for the spectral density function $J_o^{(\text{HF})}(\omega)$ as

$$J_o^{(\text{HF})}(\omega) = \frac{12\pi^2 N_M \tau_b}{d_{\text{HF}}^3} \frac{2\sigma^2 + 5\sqrt{2}\sigma + 8}{\sigma^6 + 4\sqrt{2}\sigma^5 + 16\sigma^4 + 27\sqrt{2}\sigma^3 + 81\sigma^2 + 81\sqrt{2}\sigma + 81} \quad (15)$$

where $\sigma = \sqrt{\omega\tau_b}$. Equation (15) may be substituted into Eq. (1) to yield to the relaxation rate which can be used to fit to experimental data with two fit parameters d_{HF} and diffusion time constant τ_b . As the Hwang-Freed model is a continuum model, τ_b would be expected to align with the bulk diffusion time constant for water and is labelled accordingly. A molecule of water with a diffusion coefficient of $2.3 \times 10^{-9} \text{ m}^2/\text{s}$ takes 5.3 ps to move a distance 0.27 nm (nearest neighbor distance) at room temperature²². However, the water in the outer sphere closest to the ion dominates the relaxation rate. This is the water in the second hydration layer to the ion which has restricted motion and a longer dynamical time constant. Indeed, the fits in section V yield values of τ_b greater than 5.3 ps.

The outer shell model and the continuum models for the outer-sphere water constitute two extreme representations. The outer shell model places all the water, regardless of its distance from the ion, at a precise distance d and therefore characterises the rotational dynamics but not the translational dynamics. By contrast, the continuum models captured by Eqs. (14) and (15) are derived from a model that considers only the changes in the distance between

pairs of spins and therefore consider only relative translational diffusion with rotational motion playing no role.

III. MOLECULAR DYNAMICS

The validity of the Brownian shell model introduced in section II and the appendix is tested through MD simulations. The angular probability density function $P(\beta, t)$ derived as Eq. (A6) for the rotational dynamics of the $S-I$ vector is compared to results obtained from MD simulations. The MD simulations also provide guide values for parameters obtained from the fits to experimental FFC-NMR dispersion curves for aqueous paramagnetic ions solutions in section V.

The MD computational technique involves setting up the Cartesian coordinates of the atoms in the system, defining the interatomic potentials between all the combinations of atomic species and letting the system evolve according to Newton's laws of motion. The MD simulations were performed using the Large-scale Atomic/Molecular Massively Parallel Simulator (LAMMPS) package³¹ on the High Performance Computing (HPC) facility at the University of Surrey. LAMMPS is an open-source and free MD program from Sandia National Laboratories (USA).

Initial simulations were undertaken for aqueous sodium chloride solution. This system was chosen because of the well-characterised interatomic potentials and because the singly-charged cation allows the maximum number of aquoions in a system of a given size and therefore provides the best statistics for the assessment of rotational ion-H dynamics. Subsequent simulations were undertaken on aqueous manganese(II) and iron(III) chloride solutions. Simulations were executed with periodic boundary conditions in a cubic box with side length of 100 Å. Software called Moltemplate³² was used to build the molecule and force-field database system for LAMMPS. Parameters such as mass, charge, coordinates, pair interaction parameters were specified and run in Moltemplate to generate the required database for LAMMPS to read and execute the simulation.

The SPC/E potential^{33,34} was chosen to describe the water-water interactions. The SPC/E is built from Lennard-Jones interatomic potential functions and Coulombic electrostatic interaction between partial atomic charges. This potential reproduces the self-diffusion coefficient for water to reasonable accuracy³⁵. The Lennard-Jones pairwise potential param-

eters for Na^+ and Cl^- are obtained from Joung and Cheatham³⁶ with a charge +1.0 for sodium and combined for two different atoms using the Lorentz-Berthelot combining rules. The combination with the SPC/E water potential set yields good agreement with experiment for the sodium ion diffusion coefficient³⁷. The Mn^{2+} and Fe^{3+} potentials were obtained by changing the mass and charge of the cation.

Each set of full simulations was preceded by an equilibration step. The equilibration procedure was initiated using the NPT ensemble at 300 K for 100 ps. This is a statistical mechanical ensemble that keeps the number of particles (N), pressure (P) and temperature (T) constant. The system equilibration was confirmed by the observation of the temperature and pressure fluctuating about constant values. This final configuration was taken as an input to the main simulation which was executed using the NVT ensemble. This is a canonical ensemble which places the system in a heat bath to allow exchange of energy using the Nosé-Hoover thermostat³⁸. The NVT ensemble has constant number of particles (N), volume (V) and temperature (T). The numerical integration was undertaken using a time step of 1 fs. Data collection took place at 1 ps time intervals for the NaCl simulations for a simulation length of 100 ps. This was sufficient to yield good statistical accuracy for the angular probability density function $P(\beta, t)$ for proton spins in the outer sphere of the sodium ions and a robust estimate of the outer-sphere rotational time constant $\tau_{o\beta}$.

The MD simulations of aqueous manganese chloride produce a radial distribution function for comparison with the distance fit parameters, and to obtain estimates of the rotational and exchange time constants. Two MnCl_2 simulations of duration 400 ps and 10 ns were executed with data collection every 2 ps and 100 ps respectively. The long simulation ensures that diffusivity of the (slow-moving) ion complexes can be analysed. The shorter simulation of 400 ps captures the distribution of the angle β and allows the determination of the Lévy parameter to establish the validity of the assumption of the Brownian motion of β .

IV. EXPERIMENTS

Fast-field-cycling NMR experiments were undertaken for samples of MnCl_2 , FeCl_3 and CuCl_2 at different concentrations. Initially, a 50 ± 0.06 mL of solution is prepared for each salt using deionised water at pH 7. Both the salt and water are weighed separately. The solutions are diluted to obtain 10 mL samples at the desired concentration before de-gassing

to remove dissolved paramagnetic O₂ using the freeze-thaw method as follows. A small volume of approximately 0.1 mL of solution is transferred to Ø5×220 mm Wilmad economy borosilicate NMR 100 MHz tubes. Each tube is connected to a vacuum pump with the pressure limiter pre-set to 20 kPa. The sample is frozen in liquid N₂ for 18 s and then evacuated before opening up the safety valve for 5-10 s. After the system is closed and the ice turns to liquid, the process is repeated two more times. The glass tube is sealed with a butane fuelled torch, de-greased with ethanol, then placed and centered in Ø10 mm tubes for the experiment.

A Stellar Spinmaster FFC-2000 fast field-cycling NMR relaxometer was used to acquire the frequency-dependent spin-lattice relaxation rate, $T_1^{-1} = R_1$, from solutions of MnCl₂ at 6.01, 2.00 and 0.50 mM, for FeCl₃ at 2.5 and 1.5 mM and CuCl₂ at 9.20, 3.57 and 1.50 mM. Each sample was placed in the apparatus and left for approximately 10 minutes to equilibrate to the pre-calibrated air-flow temperature of 25°C. The equipment allows the user to measure $R_1(\omega)$ at low frequency (< 0.328 T, or 14 MHz ¹H Larmor frequency, $\nu_L = \gamma B/2\pi$) using pre-polarized (PP) pulse sequences at low frequency and non-polarized (NP) pulse sequences at high frequency (> 14 MHz).

The PP sequence involves switching to a high polarization field, B_p , for a time $t_p > 5T_1(B_p)$, sufficient to maximise the initial ¹H magnetization. In this case $B_p = 0.587$ T (equivalent to 25 MHz) was used. The field is subsequently reduced to B_r for a time t_r . The switching time $t_{\text{off}} \ll T_1(B_r)$ of typically 3 ms must be sufficiently short that no magnetization is lost during the switch and B_r must subsequently be sufficiently stable that the spin system evolves during t_r according to $T_1(B_r)$, i.e. it decreases to the equilibrium value at this field. This is followed by a switch to B_a , where $B_a > B_r$, and after the field stabilises a $\pi/2$ radiofrequency pulse, resonant at ν_a (16.3 MHz in this case equal to $\gamma B_a/2\pi$), is applied which results in a free-induction decay (FID) during t_a , the integral of which is a measure of the magnetization present at the end of t_r . Following a recycle delay, RD, of several seconds at zero field, the process is repeated. Typically eight scans are used to complete an excitation pulse phase cycle and improve the signal-to-noise ratio. To measure $R_1(B_r)$ the process is repeated for, in this case, 16 different values of t_r . The FID, conventionally, is exponentially decaying at a rate of $M(t_a) = M_0 \exp(-t_a/T_2^*)$ where $1/T_2^* = 1/T_2 + 1/T_{\Delta B}$, and single exponential decay was confirmed for the samples in this study.

During a NP sequence, any initial longitudinal ¹H magnetization is ‘quenched’ by prepar-

ing the spin system at zero field for several seconds (RD) and switching then to B_r for duration t_r , during which time the magnetization increases to the equilibrium value at B_r . After switching to $B_a=0.383$ T (equivalent to 16.3 MHz which in this case typically $< B_r$), an FID is acquired as before. Similarly to PP, the cycle is repeated for different t_r values³⁹. The FFC-NMR profile $R_1(\omega)$ was acquired at typically 20 logarithmically-spaced frequencies.

V. RESULTS

Central to the shell models is the description of the rotational spin-pair dynamics captured by the time-dependent probability density function $P(\beta, t)$ in Eq. (A6). The validity of $P(\beta, t)$ is established in subsection V A. Experimental observations on the exchange lifetime τ_{ex} which are critical to the identification of appropriate inner- and outer-shell models are discussed in subsection V B. The experimental data and model fitting are then described for manganese(II), iron(III) and copper(II) respectively.

A. Validation of the probability density function

The validity of $P(\beta, t)$ given by Eq. (A6) was tested by comparison with MD simulations of aqueous NaCl solution executed as described in section III. Figure 3 shows the time-dependent probability density function $P(\beta, t) \sin \beta$ for time intervals Δt of 2, 10 and 20 ps. The product $P(\beta, t) \sin \beta$ is normalised to unity when integrated with respect to β . Only ion⁻¹H vectors for spins in the outer-sphere (taken as $r > 2\delta = 5.4 \text{ \AA}$) at both $t=0$ and at time t are included. A similar analysis of the inner sphere water is not practical as the statistical uncertainties are too large and the timescale for rotation too long to be of value.

The outer-shell model is fit to the MD probability density function for $\Delta t = 10$ ps using the Lévy parameter α and outer shell rotational time constant $\tau_{o\beta}$ as fit parameters. A simple minimisation of the squared difference Q was used to locate the optimum fit. Fits within 1% of the optimum Q yield $\alpha = 1.90 \pm 0.02$ confirming the reasonableness of the Brownian rotational motion ($\alpha = 2$) approximation for $S-I$ spin pairs in aqueous solution.

The best fit value of $\tau_{o\beta}$ at $\Delta t = 10$ ps is 30 ps. The theory curves for $\Delta t = 2$ ps and 20 ps in Fig. 3 are not fits, but use the fit parameters $\alpha = 1.9$ and $\tau_{o\beta} = 30$ ps obtained from the $\Delta t = 10$ ps dataset. The match with the equivalent MD simulation data at $\Delta t = 20$ ps is impressive establishing the validity of applying these values generally. The small systematic

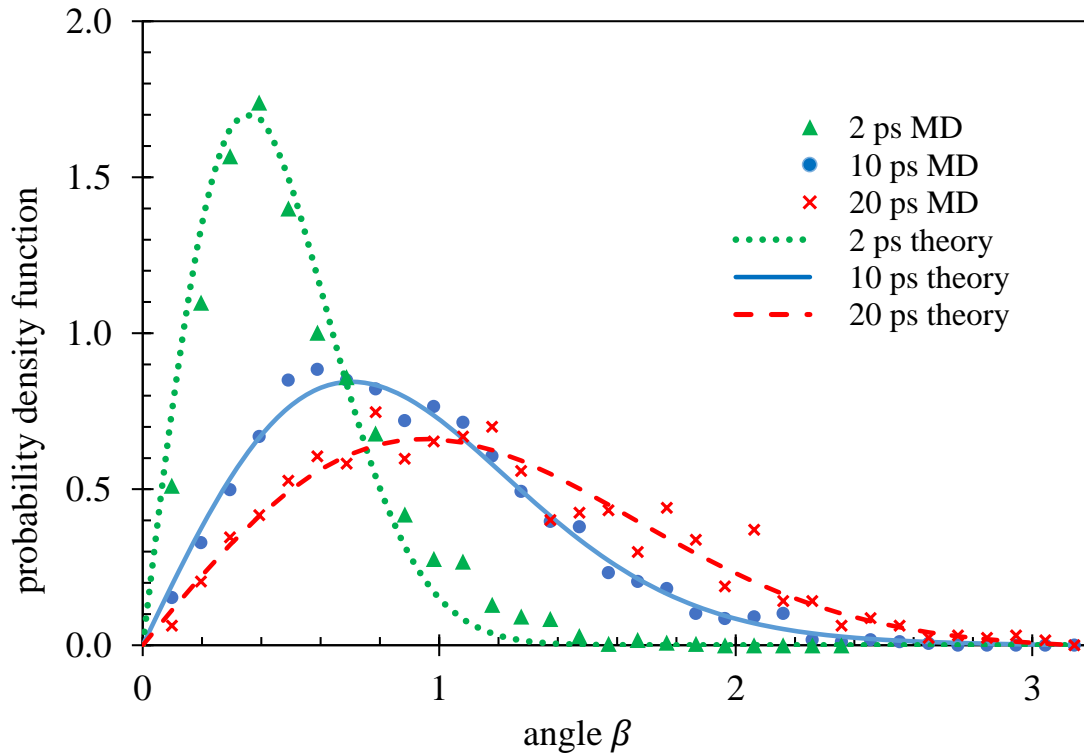
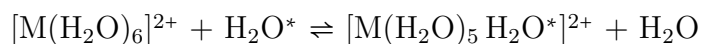


FIG. 3: The figure shows the probability density function $P(\beta, t) \sin \beta$. The data points are from MD simulations. The theory curves are obtained from Eq. (A6). The theory curve at 10 ps has been fit to the MD data using fit parameters α and $\tau_{0\beta}$ (see text). These fit parameters are used then for the theory curves at 2 ps and at 20 ps.

deviations at $\Delta t = 2$ ps are expected because, over such a small timescale, sufficient collisions have not taken place to establish Brownian statistics.

B. The exchange lifetime for aquoions

The water molecules in the inner sphere of an aquoion may exchange with a water molecule in the outer sphere and move into the bulk. The water exchange process is described by



for a metal ion M^{2+} . As noted above, the exchange time constant τ_{ex} characterises the assumed exponential decay of the number of water molecules remaining in the inner sphere after time t , $N(t)$, so that $N(t) = N_0 \exp(-t/\tau_{\text{ex}})$.

The dynamics of inner-sphere water molecules are described by quantum rather than classical mechanics²⁵ and quantum chemical calculations are necessary to predict the rate constants. Helm and Merbach²⁵ provide an excellent review of exchange mechanisms between the inner and outer sphere and gather data on exchange rates k , measured primarily by ^{17}O NMR, for a wide range of ions including the hexahydrates of Mn^{2+} , Fe^{3+} and Cu^{2+} of interest here. The reciprocal of the exchange rate is described as the mean lifetime of a water molecule in the inner sphere²⁵ so that $\tau_{\text{ave}} = k^{-1}$. Note that $\tau_{\text{ex}} = \ln(2)\sqrt{2}\tau_{\text{ave}} = 0.98\tau_{\text{ave}}$ so that $\tau_{\text{ex}} \approx \tau_{\text{ave}}$. Throughout, the equivalence of τ_{ave} and τ_{ex} is assumed.

cation complex	method	anion	τ_{ex} (s)	source
$[\text{Mn}(\text{H}_2\text{O})_6]^{2+}$	^{17}O NMR	$(\text{ClO}_4)^-$	4.8×10^{-8}	Ducommun <i>et al</i> ⁴⁰
	FFC-NMR	Cl^-	1.5×10^{-6}	this work
$[\text{Fe}(\text{H}_2\text{O})_6]^{3+}$	^{17}O NMR	$(\text{OH})^-$	6.3×10^{-3}	Swaddle <i>et al</i> ⁴¹ ; Grant <i>et al</i> ⁴²
	FFC-NMR	Cl^-	$> 1 \times 10^{-4}$	this work
$[\text{Cu}(\text{H}_2\text{O})_6]^{2+}$	^{17}O NMR	$(\text{ClO}_4)^-$	2.3×10^{-10}	Powell <i>et al</i> ⁴³
	FFC-NMR	Cl^-	2.4×10^{-10}	this work

TABLE III: The lifetime of water molecules in the inner sphere of selected aquoions are presented²⁵.

Helm and Merbach²⁵ point out that the quantum nature of the inner-sphere water dynamics leads to values of τ_{ex} ranging over 20 orders of magnitude. A water molecule might remain in the inner shell for 300 years in the case of $[\text{Ir}(\text{H}_2\text{O})_6]^{3+}$, but only 200 ps for $[\text{Eu}(\text{H}_2\text{O})_7]^{2+}$. It is not possible to predict the value of τ_{ex} for a specific ion without resorting to quantum chemical calculations. The inner-sphere water lifetime τ_{ex} depends on the energetics of transition states which in turn are critically sensitive to the electronic structure of the ion. The mean lifetime of the ions of interest are presented in table III.

C. Fitting preliminaries

Fast-field cycling NMR measurements of aqueous solutions of manganese(II), iron(III) and copper(II) chlorides were completed at m concentrations for a specific salt. The experimental relaxation rates $R_1(\omega_{ij})$ at the j^{th} of N_i frequencies ω_{ij} , where i corresponds to the i^{th} molar concentration (in units of mM), were converted to a 1 mM master relaxation rate $R_1^{(1)}(\omega_{ij})$, sometimes referred to as a relaxivity, using the equation

$$R_1^{(1)}(\omega_{ij}) = \frac{R_1(\omega_{ij}) - R_{1,\text{offset}}}{c_i} \quad (16)$$

where c_i is the concentration used for the scaling.

The frequency- and concentration-independent offset relaxation rate $R_{1,\text{offset}}$ is found by minimising

$$Q = \sum_{j=1}^{N_i} \sum_{i=1}^m \left[R_1^{(1)}(\omega_{ij}) - \langle R_1(\omega_{ij}) \rangle_i \right]^2 \quad (17)$$

where the angular brackets indicate an average over concentrations $i = 1 \dots m$. $R_{1,\text{offset}}$ accounts for frequency-independent contributions *not* associated with dipolar S - I interactions, such as proton-proton interactions, residual contributions due to impurities or un-removed dissolved dioxygen, and electron spin relaxation. Furthermore, relaxation rates are not necessarily directly proportional to concentration at high paramagnetic ion concentrations presumably due to interactions between hydrated-ion complexes.

The values of $R_{1,\text{offset}}$ and c_i used for each ion are listed in table IV. In the case of aqueous CuCl_2 , measurements at $m=3$ different concentrations are scaled using the actual ion concentration. The Q is minimised with a physically-reasonable offset of 0.43 s^{-1} . By contrast, in the case of Mn^{2+} , it was necessary to minimise Q by changing both the highest scaling concentration and $R_{1,\text{offset}}$ leading to a scaling concentration of 5.56 mM compared to the experimental concentration of 6.01 mM and an offset of 0.70 s^{-1} . For Fe^{3+} , minimising Q with respect to $R_{1,\text{offset}}$ only yields the unphysical result $R_{1,\text{offset}} = 0 \text{ s}^{-1}$. $R_{1,\text{offset}}$ must exceed the spin-lattice relaxation rate for pure water at room temperature⁴⁴, which is about 0.28 s^{-1} . A typical estimated value of 0.4 s^{-1} was set. Q was then minimised with respect to the highest scaling concentration to yield 2.9 mM compared to the experimental concentration of 2.5 mM .

	Mn^{2+}			Fe^{3+}		Cu^{2+}		
Experimental ion concentrations (mM)	6.01	2.0	0.5	2.5	1.5	9.2	3.57	1.5
Scaling concentration c_i (mM)	5.56	2.0	0.5	2.9	1.5	9.2	3.57	1.5
Offset relaxation rate $R_{1,\text{offset}}$ (s^{-1})	0.70			0.4*		0.43		

TABLE IV: Sample ion concentrations and scaling parameters for each aquoion. Both the scaling concentration c_i and offset rate $R_{1,\text{offset}}$ are used in Eq. (16). The * indicates an estimated offset (see text).

Three alternative outer-sphere models illustrated in Fig. 2(b)-(d) were assessed. Each was combined with the inner-sphere shell model and fit to the dispersion data described in

		Mn ²⁺	Fe ³⁺	Cu ²⁺
Electronic spin quantum number	S	$\frac{5}{2}$	$\frac{5}{2}$	$\frac{1}{2}$
Number of inner-sphere proton spins	n	12	12	5
Constant in Eq. (1)	β_{IS}	$2.47 \times 10^{11} S(S+1) \text{ m}^6 \text{ s}^{-2}$		
Paramagnetic ion density (1 mM)	N_M	$6.02 \times 10^{-4} \text{ ions/nm}^3$		
Bulk water spin density (1 mM)	N_H	66.6 spins/nm^3		

TABLE V: Numerical values of physical quantities used in calculations. The $n=12$ corresponds to six inner-sphere water molecules as expected, the Cu²⁺ case is discussed in section VF.

	inner sphere		outer sphere	
	shell		shell	Hwang-Freed
	a, τ_{ex}	$a, \tau_{i\beta}$	$d, \tau_{o\beta}$	$d_{\text{HF}}, \tau_{\text{b}}$
Mn ²⁺	✓	✓	✓	✓
Fe ³⁺	✓	✓	✓	✓
Cu ²⁺	✓		✓	

TABLE VI: Model combinations presented and discussed in sections VD to VF.

the following sections. The quality of fit was assessed by the coefficient Q given by

$$Q = \sum_{j=1}^{N_i} \sum_{i=1}^n \left[R_1^{(1)}(\omega_{ij}) - R_1^{(\text{model})}(\omega_{ij}) \right]^2 \quad (18)$$

where $R_1^{(\text{model})}(\omega_{ij})$ is the prediction of the chosen model at the j^{th} frequency (ω_{ij}) for each of the i normalised datasets. The equations for all models used to fit to the experimental dispersion data are presented in section IIB and in the appendix for the shell model. The values of physical quantities used are presented in table V.

All combinations of inner- and outer-sphere models were explored during the fitting process. The model combinations with the best fits are discussed in detail in the following sections and are presented in summary in table VI.

D. Manganese

The first frequency-dependent T_1 data for a dilute aqueous manganese ion system were presented by Morgan and Nolle in 1959¹¹. More recently, literature field-cycling measurements for Mn²⁺ for a range of anions are summarised and interpreted in Chapter 7 of the

book by Bertini *et al*³.

Here, FFC-NMR relaxation rate measurements on aqueous MnCl_2 solutions at concentrations 0.5, 2.0, and 6.01 mM are presented. The data are transformed into a 1 mM master curve as described in section VC and presented in Fig. 4.

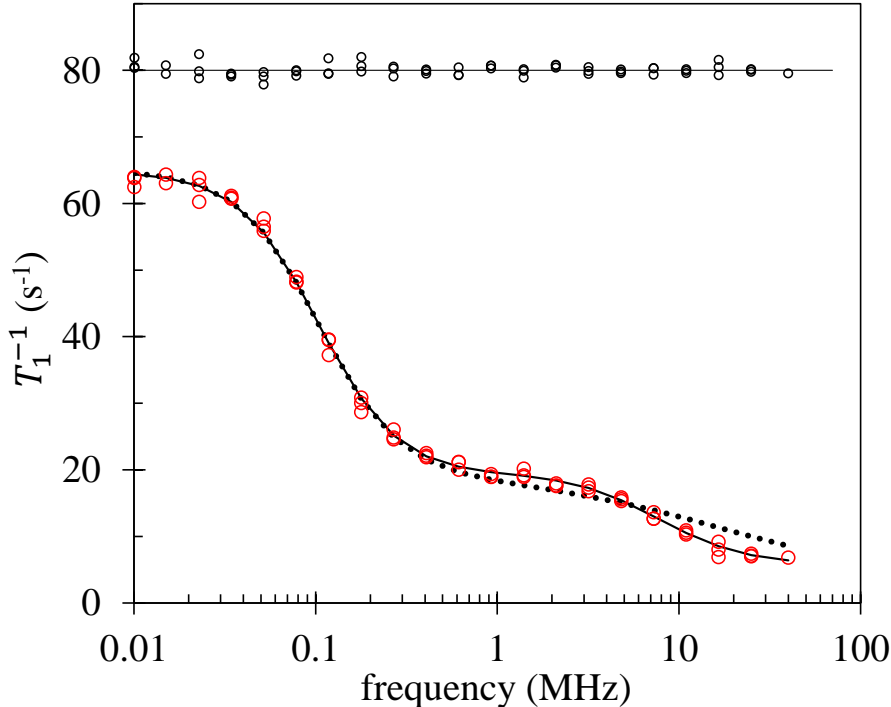


FIG. 4: Experimental FFC-NMR data for aqueous manganese chloride solution (\circ) scaled to 1 mM (see text) are presented. The best fit $\text{shell}(\tau_{\text{ex}})+\text{shell}(\tau_{0\beta})$ model combination is shown by the solid line with residual offsets (\circ). The $\text{shell}(\tau_{1\beta})+\text{Hwang-Freed}$ best fit is presented as a dotted line.

Manganese(II) presents two inflection features at about 0.1 and 10 MHz which are associated with water in the inner and outer spheres respectively¹³. Two versions of the shell model describe the inner-sphere contribution to the relaxation rate. One version assumes $\tau_{1\beta} \gg \tau_{\text{ex}}$ so that the exchange time constant τ_{ex} dominates the relaxation. The inner sphere water exchanges with outer sphere water faster than the rate of rotation of the ion complex. This version of the inner-sphere shell model uses the fit parameter set (a, τ_{ex}) and is referred to as $\text{shell}(\tau_{\text{ex}})$. The second version of the inner-sphere shell model takes $\tau_{1\beta} \ll \tau_{\text{ex}}$ and uses the fit parameter set $(a, \tau_{1\beta})$. Here, rotation of the ion complex is faster than the exchange

lifetime and is abbreviated to shell($\tau_{i\beta}$).

Each inner-sphere shell model was explored in tandem with one of the outer-sphere models illustrated in Fig. 2(b)–(d). The continuous diffusion model illustrated in Fig. 2(c), requires the numerical calculation of the dipolar correlation function $G(t)$ given by Eq. (14) followed by a second numerical integration to execute the Fourier transform to finally obtain the spectral density function $J(\omega)$. The continuous diffusion model is not discussed further because the Hwang-Freed model in Fig. 2(d) not only provides an improved physical description of the bulk diffusion of fluid in the vicinity of an ion and the convenience of an analytic expression for $J(\omega)$, but in trial fits was also found to provide a superior fit to the experimental data. The Hwang-Freed outer-sphere model uses the parameter set ($d_{\text{HF}}, \tau_{\text{b}}$), where τ_{b} is the water bulk diffusion time constant. The second outer-sphere model is the shell($\tau_{o\beta}$) model with parameter set ($d, \tau_{o\beta}$).

		Fit-Mn1	Fit-Mn2	Fit-Mn3
Inner sphere model:		shell(τ_{ex})	shell($\tau_{i\beta}$)	shell(τ_{ex})
radius of inner shell	a	0.272 nm	0.263 nm	0.270 nm
exchange time constant	τ_{ex}	1.5 μs		1.5 μs
rotational time constant (inner)	$\tau_{i\beta}$		1.8 μs	
Outer sphere model:		shell	shell	Hwang-Freed
radius of outer shell	d	0.446 nm	0.435 nm	
rotational time constant (outer)	$\tau_{o\beta}$	37 ps	32 ps	
Hwang-Freed distance	d_{HF}			0.408 nm
bulk diffusion time constant	τ_{b}			27 ps
inner sphere volume fraction	x	3.67×10^{-5}	3.38×10^{-5}	3.47×10^{-5}
quality-of-fit parameter	Q	39.5	52.5	134

TABLE VII: The table presents the best fit parameters for the relaxation rate dispersion from aqueous manganese chloride solution for three alternative models.

The optimum fit parameters for three of the four model combinations are presented as Fit-Mn1, Fit-Mn2 and Fit-Mn3 in table VII. The dispersion curves for Fit-Mn1 and Fit-Mn3 are displayed in Fig. 4 (the curves for Fit-Mn1 and Fit-Mn2 are very similar). The dispersion curves coincide at frequencies less than about 0.2 MHz because both Fit-Mn1 and Fit-Mn3 use the same inner-sphere model and it is the inner-sphere model that characterises the low-frequency region of the dispersion curve. By contrast, there is a significant difference at frequencies above 1 MHz with shell($\tau_{o\beta}$) significantly outperforming the Hwang-Freed model.

The fit parameters presented in table VII are compared to MD simulations of aqueous manganese chloride. The Mn^{2+} -H radial distribution function $\rho(r)/\rho_0$ obtained from a MD

simulation of aqueous MnCl_2 is presented in Fig. 5 where ρ_0 is the density of H atoms in bulk water. The Mn^{2+} aquoion forms a hexahydrate and the MD simulation also shows six water molecules in the first coordination shell. The Mn^{2+} -H radial distribution function shows a sharp peak close to the fit value confirming that the shell approximation is good for the inner sphere.

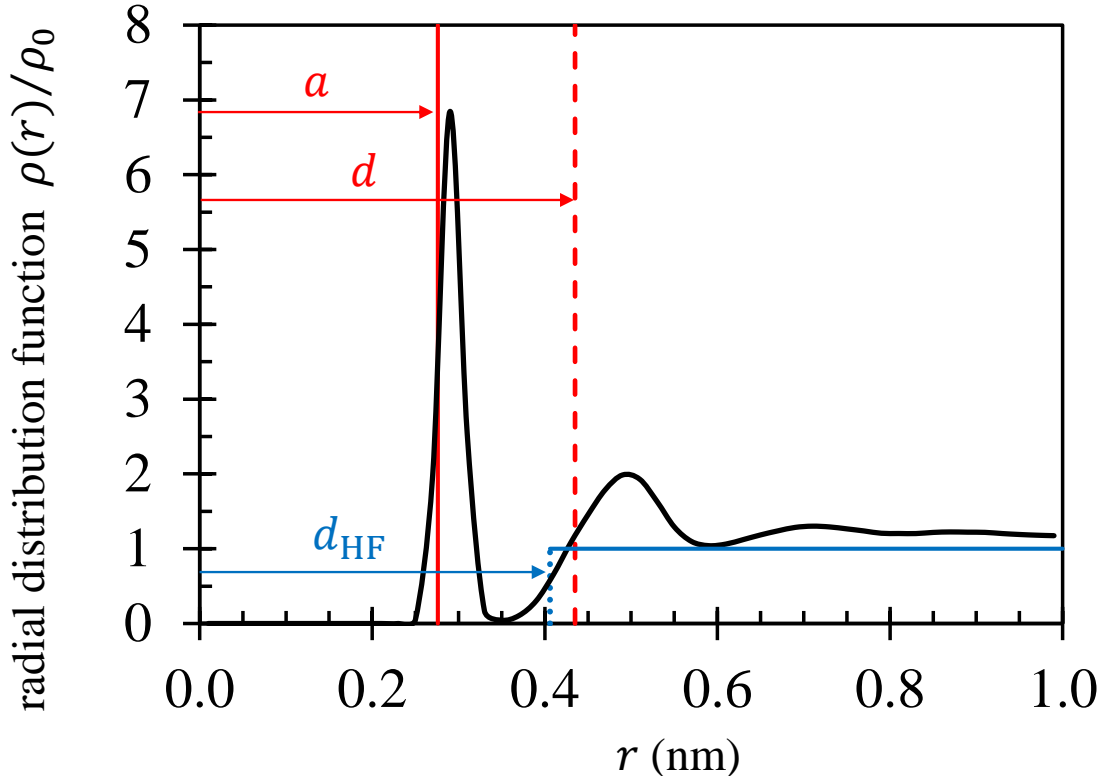


FIG. 5: The Mn^{2+} -H radial distribution function obtained from a MD simulation of aqueous MnCl_2 is presented. The shell model radii a and d , and the Hwang-Freed distance of nearest approach d_{HF} are shown as obtained from fits to the experimental relaxation rate dispersion curve for aqueous MnCl_2 .

The best-fit shell-model radii a and d , and the Hwang-Freed distance d_{HF} listed in table VII are shown in Fig. 5. The values of a fall in a narrow range 0.263–0.272 nm. The middle value is shown and is in very good agreement with the peak of the first coordination shell from MD simulation. The inner shell radius a can also be compared to experimental results of Smirnov and Grechin⁴⁵ who used X-ray diffraction to determine the radial distribution functions for aqueous MnCl_2 solutions for a range of concentrations. The evolution of the radial distribution function for four different concentrations was presented demonstrating

the sharpening of the first coordination shell as the salt solution became increasingly dilute. Unfortunately, the lowest concentration studied is still substantially higher than 1 mM for the FFC-NMR measurements presented here. Nonetheless, table 1 of Smirnov and Grechin⁴⁵ shows that the Mn²⁺-O distance is nearly independent of concentration at about 0.216 nm. Taking this value and assuming that the oxygen atom of the water molecule is pointing towards the manganese ion and the H atoms away from the ion, and using the O-H bond length of 0.096 nm and a H-O-H angle of 104.5°, the H atoms are placed 0.275 nm from the center of the manganese ion. The agreement with the range of values of a obtained presented in table VII is impressive. Moreover, the relaxation rate is proportional to r^{-4} so that the best-fit a would be expected to lie at a distance slightly less than the peak of the radial density function. This result provides confidence in the shell model presented in section II as a quantitative description of the inner-sphere water dynamics.

The best-fit outer-shell radius d is shown in Fig. 5 for comparison with the second hydration peak of the radial distribution function. As for a , the r^{-4} distance-dependence of the relaxation rate suggests d would fall on the side of the second hydration peak closest to the origin. The Hwang-Freed model yields a best-fit time constant $\tau_b = 27$ ps. As anticipated in section II B 2, this value represents a diffusion coefficient a factor of five smaller than for pure water at room temperature²². The time constant reflects the slower motion of water in the second coordination shell and the strong distance dependence of the relaxation rate will therefore over-weight the contribution of the water in this region. Similarly, fits to FFC-NMR dispersion curves from porous systems typically yields τ_b in the range 10–20 ps¹⁷, approximately three times longer than for pure water at room temperature, an outcome consistent with MD simulation³⁰. The fit time constant $\tau_b = 27$ ps from Fit-Mn3 is consistent with these observations.

The best-fit values of the rotational time constant for the outer shell, $\tau_{o\beta}$, are 37 ps and 32 ps. A guide value for $\tau_{o\beta}$ is easily calculated from the MD simulations of MnCl₂ described in section III whereupon a value of 32 ps is obtained. These outcomes are in good agreement with the experimental value of 29 ps was found by Koenig and Brown⁴⁶ for aqueous manganese(II) at 35°C.

The best-fit value of τ_{ex} of 1.5 μ s from Fit-Mn1 and Fit-Mn3 is a factor of about 30 longer than the mean water exchange lifetime obtained from ¹⁷O NMR measurements of Ducommun and co-workers⁴⁰, albeit with a different anion. Unfortunately, MD simulations

are unable to provide a guide value for $\tau_{i\beta}$, primarily because the inner-shell hydrate water exchanges with the second coordination shell too rapidly. However, Hernández and Bryant⁴⁷ find $\tau_{i\beta} \approx 10 \mu\text{s}$ for a manganese porphine complex, which is satisfyingly close to the value obtained here considering the relative physical sizes of the complexes.

The optimum combination of models for aqueous manganese chloride solution is shell(τ_{ex}) + shell($\tau_{o,\beta}$) as Fit-Mn1, although shell($\tau_{i,\beta}$) + shell($\tau_{o,\beta}$) in Fit-Mn2 also yields an excellent fit suggesting that $\tau_{\text{ex}} \approx \tau_{i,\beta}$ for the manganese system. The combinations yields fit parameters that are physically justifiable and consistent with MD simulation results or independent measurements where available.

E. Iron

Measurements of T_1 for a range of frequencies from aqueous iron (III) were presented by Bertini and co-workers in 1993⁴⁸. These authors added perchloric acid to avoid the formation of hydroxide precipitates. Field-cycling data for iron (III) with various anions are summarised by Bertini *et al*¹³. Iron (III) is a common impurity in a range of porous material and aqueous iron (III) may desorb into the pore water, contributing to the measured NMR relaxation rates.

Here, the FFC-NMR dispersion curves for an aqueous solution of iron(III) chloride at 1.5 mM and 2.5 mM were converted to a master 1 mM curve with an assumed offset of 0.4 s^{-1} (see table V) and displayed in Fig. 6. Iron is next to manganese in the periodic table and both Fe^{3+} and Mn^{2+} have the same number of electrons. Nevertheless, its dispersion curve is fundamentally different from that of aqueous manganese chloride solution. The data reveal a single inflection at a frequency of about 10 MHz, presumably associated with the interaction of Fe^{3+} with fast-moving (outer sphere) ^1H spins. The sudden increase in relaxation rate at 40 MHz is a feature of aqueous iron(III) systems^{48,49}. Bertini *et al*⁴⁸ suggest that the feature is consistent with electronic spin relaxation with a time constant of a few picoseconds. These two data points are excluded from the fits.

Table III shows that the lifetime of a water molecule in the $[\text{Fe}(\text{H}_2\text{O})_6]^{3+}$ complex is long, of order milliseconds. Therefore $\tau_{\text{ex}} \gg \tau_{i\beta}$ and the inner-sphere contribution to the dispersion curve is dominated by the rotational time constant $\tau_{i\beta}$. However, there is no obvious inflection feature indicative of relaxation of inner-sphere water in the frequency

range of the experiment.

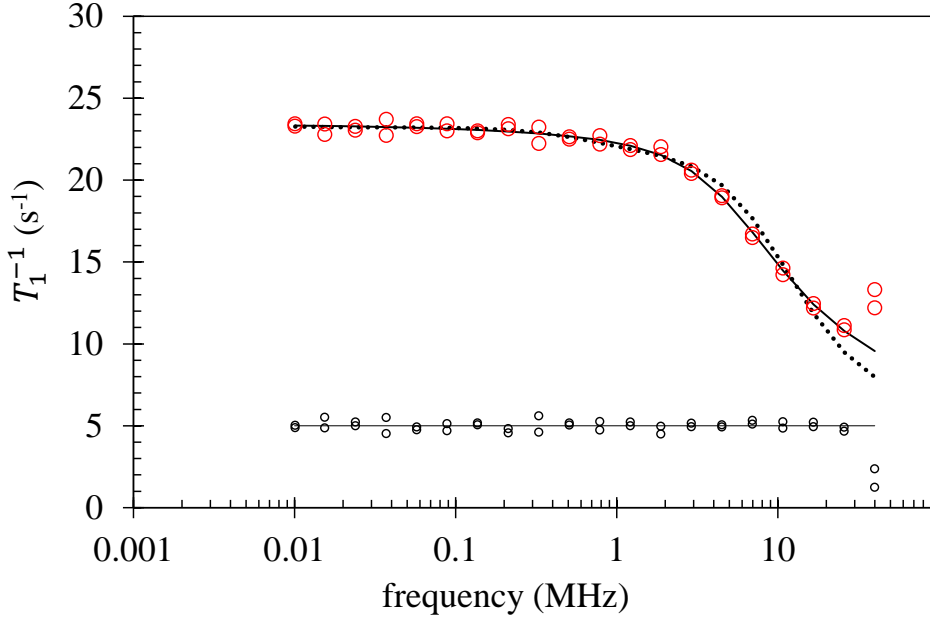


FIG. 6: The experimental relaxation rate dispersion curve for aqueous iron(III) chloride solution (○) scaled to 1 mM is presented. The shell($\tau_{o,\beta}$)+Hwang-Freed (Fit-Fe1) model fit combination is shown by the solid line with residual offsets (○). The dotted line is the shell($\tau_{i,\beta}$)+shell($\tau_{o,\beta}$) model combination (Fit-Fe2). The origin of the two highest-frequency data points is discussed in the text.

The fit outcomes for two model combinations, labelled Fit-Fe1 and Fit-Fe2, are presented in Fig.6 and table VIII. Fit-Fe1 assumes that inner-sphere relaxation is not seen in the dispersion curve because the water exchange lifetime τ_{ex} and rotational time constant $\tau_{i\beta}$ are both too long to be observed in the frequency range of the experiment. Therefore the relaxation rate dispersion across the full frequency range is considered to arise solely due to interactions of the paramagnetic ion with the water in the outer sphere. Neither the shell($\tau_{o,\beta}$) nor Hwang-Freed model alone provide a satisfactory fit to the dispersion curve, but a combination of the two models provides an excellent fit. The parameter sets ($d, \tau_{o\beta}$) and (d_{HF}, τ_b) are presented as Fit-Fe1 in table VIII. Both the shell($\tau_{o,\beta}$) and Hwang-Freed models apply to the outer sphere, so that x represents the fraction of spins contributing to the shell model leaving the fraction $1 - x$ of spins contributing to the Hwang-Freed model. The outer-shell rotational time constant $\tau_{o\beta}$ obtained from Fit-Fe1 is 37 ps consistent with 30 ps reported by Bertini and co-workers⁴⁸ albeit through a different relaxation mechanism.

The outer-shell radius d in Fit-Fe1 is consistent with a second hydration peak and the Hwang-Freed distance of nearest approach is shorter at 0.343 nm, again as expected. The bulk diffusion time constant $\tau_b = 15$ ps is exactly in the expected range 10–20 ps.

		Fit-Fe1	Fit-Fe2
Inner sphere model:			shell($\tau_{i\beta}$)
radius of inner shell	a		0.176 nm
rotational time constant (inner)	$\tau_{i\beta}$		0.12 μ s
Outer sphere model:		shell + HF	shell
radius of outer shell	d	0.406 nm	0.381 nm
rotational time constant (outer)	$\tau_{o\beta}$	37 ps	21 ps
Hwang-Freed distance	d_{HF}	0.343 nm	
bulk diffusion time constant	τ_b	15 ps	
inner sphere volume fraction	x		3.64×10^{-6}
outer shell fraction	x	0.464	
quality-of-fit parameter	Q	2.66	9.4

TABLE VIII: The table presents the best fit parameters for the relaxation rate dispersion for two alternative models for aqueous iron(III) chloride solution.

Despite the success of fit Fit-Fe1, an alternative fit Fit-Fe2 is attempted which assumes that an inner sphere contribution exists. Here, it is assumed that $\tau_{\text{ex}} \gg \tau_{i\beta}$ so that $\tau_{i\beta}$ is the dominant time constant characterising the inner sphere contribution. A trial shell($\tau_{i\beta}$) + Hwang-Freed combination provided a poor quality of fit but a reasonable fit was found for the shell($\tau_{i\beta}$) + shell($\tau_{o\beta}$) model combination and the fit parameters are listed as Fit-Fe2. However, the Fit-Fe2 fit parameters are not consistent with experiment. Magini and Ragnai⁵⁰ undertook X-ray diffraction studies of aqueous iron(III) chlorides and noted that the peak position of the radial distribution function for the Fe-O distance for the $[\text{Fe}(\text{H}_2\text{O})_6]^{3+}$ complex was 0.2 nm. However, for iron(III) chlorides, this peak position is extended to 0.22–0.23 nm indicating “inner complex formation between iron and chloride”⁵⁰ and the consequential displacement of the inner sphere water O atoms to longer distances. Making the normal adjustment to determine the distance of the shell of ^1H spins from the iron center suggests a Fe-H probability maximum at 0.28–0.29 nm, in marked disagreement with 0.176 nm listed as Fit-Fe2 of table VIII. Moreover, $\tau_{i\beta} = 0.12 \mu\text{s}$ for Fit-Fe2 suggests a much faster rotating iron(III) complex compared to the manganese(II) aquoion in Fit-Mn2 of table VII, an outcome that seems unlikely.

In summary, fit Fit-Fe1 is the model of choice for aqueous iron(III) chloride. There is

no inner-sphere contribution seen in the frequency range of the experiment. An estimate of the implied lower bound value of $\tau_{i\beta}$ was made by undertaking trial fits that added a shell($\tau_{i\beta}$) component to Fit-Fe1 and assessing the quality-of-fit. The trial fits reveal that $\tau_{i\beta}$ is invisible over the frequency range of the experiment if $\tau_{i\beta} \gtrsim 100 \mu\text{s}$. Such a long rotational time constant for a hexahydrate ion complex suggests that the complex must be physically larger than its manganese(II) counterpart where $\tau_{i\beta} \approx 2 \mu\text{s}$. This observation is consistent with the assertion that chloride anions join the inner sphere increasing the physical size and mass of the complex thereby slowing its rate of rotation. Nitrate anions (from the nitric acid added to prevent precipitation of hydroxides) may also play a role.

F. Copper

Morgan and Nolle completed frequency-dependent measurements of T_1 for a dilute aqueous copper(II) in 1959¹¹ and, in 1964, Hausser and Noack identified the single inflection feature as due to dipolar interactions⁵¹. Here, fast field-cycling NMR measurements on aqueous copper(II) chloride solution were obtained at concentrations 9.2, 3.57 and 1.5 mM. The 1 mM master curve was obtained using Eq. (18) as described previously. The scaled data are presented in Fig. 7.

Table III reports that the water exchange lifetime τ_{ex} in an aqueous copper(II) chlorate complex is just 230 ps⁴³. The inner-shell water is very weakly bound, indeed one of the most weakly bound of all aquoions²⁵. Bell and co-workers⁵² undertook X-ray studies of aqueous copper chloride and concluded that Cu^{2+} ions displace some water in the inner sphere. The ion has six nearest neighbours of which, on average, 3.5 are chloride ions and about 2.5 are (water) oxygen⁵². Magini⁵³ agrees that the Cu^{2+} ion contains about 2.5 water molecules in the first coordination shell, but disputes the number of chloride ions. Exploratory fits using $n=12$ (as for Mn^{2+} and Fe^{3+} previously) did not yield time constants and distance parameters consistent with experiment. The inner-shell proton number $n=5$ is therefore used for the fits for the Cu^{2+} ion as indicated in table V. The particle radial distribution function⁵³ shows a number of broad peaks without evidence of a sharp first or second coordination shell. This supports the ¹⁷O NMR evidence of weak bonding and an unusually short residence time for water in the first coordination shell of a Cu^{2+} ion⁴³ regardless of its anion.

On this basis of the experimental evidence, it can be assumed with confidence that $\tau_{i\beta} \gg$

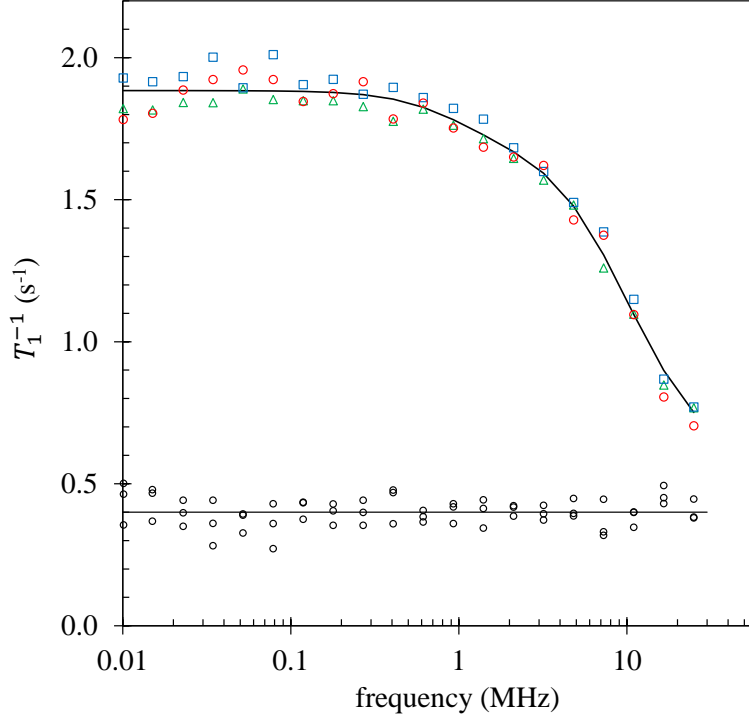


FIG. 7: The experimental relaxation rate dispersion curve for aqueous copper(II) chloride solution scaled to 1 mM from 1.5 mM (\circ), 3.57 mM (\square) and 9.2 mM (\triangle) is presented. The best fit shell(τ_{ex})+shell($\tau_{\text{o}\beta}$) combination is shown by the solid line with residual offsets (\circ).

τ_{ex} so that the inner shell contribution to the relaxation rate is dominated by the exchange lifetime τ_{ex} . The Hwang-Freed continuum model was tested but a satisfactory fit could not be obtained. By contrast, the shell($\tau_{\text{o}\beta}$) model yielded an excellent fit. Consequently, the results of the shell(τ_{ex}) + shell($\tau_{\text{o}\beta}$) combination only is presented in table IX.

Inner sphere model:		shell(τ_{ex})	shell(τ_{ex})
radius of inner shell	a	0.180 nm	0.162–0.252 nm
exchange time constant (inner)	τ_{ex}	240 ps	230–370 ps
Outer sphere model:		shell	shell
radius of outer shell	d	0.419 nm	0.413–0.419 nm
rotational time constant (outer)	$\tau_{\text{o}\beta}$	27 ps	24–27 ps
inner sphere volume fraction	x	11.2×10^{-4}	6.2×10^{-4} – 35.6×10^{-4}
quality-of-fit parameter	Q	0.142	0.142–0.149

TABLE IX: The table presents the best fit parameters for the relaxation rate dispersion for aqueous copper(II) chloride solution..

The best fit dispersion curve is presented in Fig. 7 using optimum fit parameters presented in the first column of table IX. The agreement between $\tau_{\text{ex}} = 240$ ps from the fit and 230 ps for τ_{ex} as measured by Powell and co-workers⁴³ is excellent. The rotational time constant for the outer shell at 27 ps is consistent with the manganese system.

In contrast to the iron(III) and manganese(II) systems, significant changes in x and the inner shell parameters provide only a small change (5%) in the quality-of-fit parameter. Good-quality fits can be obtained for a spread of values of x , a and τ_{ex} . The best-fit value of a of 0.18 nm is shorter than the spread of the first coordination shell observed experimentally of about 0.22–0.25 nm⁵³ but the spread of inner-shell radii presented in the second column of table IX spans the experimental range. The value of x is significantly larger than that seen for either the manganese or iron, suggesting a broad Cu–¹H radial distribution function consistent with experiment⁵³.

VI. SUMMARY AND CONCLUSIONS

Molecular dynamics simulations of aquoions confirm that the ion-¹H vector executes, to a good approximation, Brownian rotational dynamics. A shell model describing the Brownian rotational dynamics of ion-¹H spin-pair vectors of fixed length is presented and used to calculate the spin-lattice relaxation rate $R_1(\omega)$ for manganese(II), iron(III) and copper(II) aquoions. The Brownian shell model is fully-quantitative, rigorously includes the angular boundary conditions, and therefore constitutes an enhancement to the SBM model. The time-dependent dipolar correlation function describing the rotational dynamics of spin-pairs is expressed as an exponential series which can be curtailed at two terms providing an analytic expression for the frequency dependence of the spin-lattice relaxation rate $R_1(\omega)$ which is as easy to apply as the traditional SBM model.

The Brownian shell model can be applied to both the inner- and outer-sphere water. Combinations of shell models and/or the Hwang-Freed continuum model for the outer sphere can be used to provide fully-analytic, quantitative fits to experimental FFC-NMR $R_1(\omega)$ dispersion curves over the full experimental frequency range for solutions of paramagnetic salts or liquids containing paramagnetic ions in the fast-diffusion regime.

Fits to FFC-NMR relaxation rate dispersion curves over the frequency range 0.01–25 MHz are executed for aqueous manganese(II), iron(III) and copper(II) chloride solutions. Various

model combinations are tested and excellent fits are obtained for each salt. The exchange lifetime is found to play a pivotal role in determining the shape of the relaxation rate dispersion curves and dictates which combination of inner- and outer-shell models is appropriate in each case. The optimum fit parameters are presented in tables VII, VIII and IX with numerical values justified via MD simulations or by comparison with experimental data from the literature. The inclusion of additional relaxation mechanisms, such as electronic spin relaxation, is not required.

The optimum fit parameters for each of the manganese(II), iron(III) and copper(II) chloride systems yield the $R_1(\omega)$ dispersion curve as a linear function of the paramagnetic ion concentration using the equations in section II. These may be used to estimate the concentrations of manganese(II), iron(III) and copper(II) ions in mixed liquids such as wine or vinegar, or to allow the “background” contribution to the $T_1^{-1}(\omega)$ dispersion curve obtained from many porous materials to be subtracted out.

Acknowledgment

This work has received funding from the European Union Horizon 2020 Research and Innovation Programme under the Marie Skłodowska-Curie Innovative Training Networks programme grant agreement No. 764691.

Conflict of interest

The authors have no conflicts to disclose.

Data Availability Statement

The data that support the findings of this study are available from the corresponding author upon reasonable request.

Appendix A

The calculation of the inner-sphere contribution to the relaxation rate for the interaction between the electronic spin of the paramagnetic ions (S) and water proton spins (I) in a coordination shell starts with the standard expression for the dipolar correlation function presented as Eq. (A1)^{18,19}

$$G(t) = \left\langle \frac{P_2(\cos \beta)}{r_0^3 r^3} \right\rangle \quad (\text{A1})$$

where $P_2(x) = \frac{1}{2}(3x^2 - 1)$ is the second-rank Legendre polynomial and β is the smallest angle between a spin-pair vector \mathbf{r}_0 at $t=0$ and \mathbf{r} at a later time t as illustrated in Fig. 1. $G(t)$ captures all the relevant dynamical information describing how pairs of spins move relative to each other. Introducing a space- and time-dependent probability density function yields an equivalent expression

$$G(t) = \int_{\mathbb{R}^3} \int_{\mathbb{R}_0^3} \frac{P_2(\cos \beta)}{r_0^3 r^3} P(\mathbf{r}, t \cap \mathbf{r}_0) d^3 \mathbf{r}_0 d^3 \mathbf{r} \quad (\text{A2})$$

where $P(\mathbf{r}, t \cap \mathbf{r}_0)$ is the probability density function describing the probability distribution of pairs of spins separated by \mathbf{r}_0 at $t = 0$ and by \mathbf{r} at time t . The subscript 0 on all quantities indicates the value at $t = 0$. $P(\mathbf{r}, t \cap \mathbf{r}_0)$ may be expanded as

$$P(\mathbf{r}, t \cap \mathbf{r}_0) = P(\mathbf{r}_0)P(\mathbf{r}, t | \mathbf{r}_0) \quad (\text{A3})$$

where $P(\mathbf{r}, t | \mathbf{r}_0)$ is the time-dependent conditional probability density function describing a spin pair separated by \mathbf{r} at time t given that the same pair were separated by \mathbf{r}_0 at $t = 0$. $P(\mathbf{r}_0)$ is the *a priori* probability density describing the probability per unit volume of finding a spin pair, equivalent to the reciprocal of the “volume per paramagnetic spin” equal to N_M , the number of paramagnetic ions per unit volume.

A shell model demands that the $S-I$ distance is constant so that $|\mathbf{r}| = |\mathbf{r}_0| = a$, and $P(r_0) = N_M \delta(r_0 - a)$. Since $\beta = 0$ at $t = 0$, both \mathbb{R}_0^3 and \mathbb{R}^3 integrals can be executed, save for the integral involving β yielding

$$G(t) = \frac{4\delta N_M}{a^4} \int_0^\pi P_2(\cos \beta) P(\beta, t) \sin \beta d\beta. \quad (\text{A4})$$

A numerical Fourier transformation of Eq. (A4) yields the spectral density function $J(\omega)$ and then the relaxation rate $R_1(\omega)$ as described in the main text. The distance δ is the

effective thickness of the shell at radius a and appears when volume integrals are undertaken over an areal distribution of spin, such as that leading to Eq. (A4). Normally, $\delta=0.27$ nm is assumed as the mean distance between water molecules or, equivalently, the thickness of a layer of water at a surface⁵⁴. This would be an appropriate choice for the outer-sphere water which is at the bulk water density, but inappropriate for the tightly-bound inner-sphere water with a known (or assumed) areal spin density that may differ from the normal bulk density.

The inner-shell volume is considered to extend from $r = a \pm \delta/2$ and to contain n proton spins. The δ is chosen so that the inner-shell volume contains spins at the normal bulk-water density of $N_H = 66.6$ spins/nm³. At $t=0$, the dipolar correlation function $G(0) = n/a^6$ and elementary mathematics yields

$$\delta = \left[a^2 + \frac{n}{2\pi a N_H} \right]^{1/2} - a. \quad (\text{A5})$$

An expression for $P(\beta, t)$ for an anomalous (Lévy) rotor has been derived as (see supplementary material of reference¹⁴)

$$P_L(\beta, t) = N(t) \left[1 + 2 \sum_{p=1}^{\infty} e^{-p^\alpha t/\tau} \cos p\beta \right] \quad (\text{A6})$$

where α is the Lévy coefficient. The time constant τ is an rotational diffusion time constant such that $\tau/2$ is the time taken for a rotor to move through an angle of one radian¹⁴. $N(t)$ is a time-dependent normalisation constant which ensures that

$$\int_0^\pi P_L(\beta, t) \sin \beta d\beta = 1 \quad (\text{A7})$$

leading to

$$N(t) = \frac{1}{2} \left[1 - 2 \sum_{p=2,4,\dots}^{\infty} \frac{e^{-p^\alpha t/\tau}}{(p^2 - 1)} \right]^{-1}. \quad (\text{A8})$$

Symmetric Lévy processes are characterised by so-called “fat” tails, often called Pareto tails, described by a power law rather than the exponential decay characteristic of the Gaussian probability density function. The more extreme events occur more frequently than expected from a Gaussian distribution. The Lévy distribution is widely used in numerous disciplines and can be considered a generalized symmetric distribution. For example, Lévy distributions are widely used in the finance sector to describe the large fluctuations in stock prices of importance in risk assessment. Equation (A6) was introduced by Faux *et al*¹⁴ to

describe the large, sudden changes in angle of the intra-molecular $^1\text{H}-^1\text{H}$ vector for water associated with hydrogen-bond breaking and reforming. The “fatness” of the tails is determined by the Lévy coefficient α where $0 < \alpha \leq 2$. The limits $\alpha = 2$ and $\alpha = 1$ correspond to Gaussian and Cauchy-Lorentz distributions respectively.

In the present article, the Lévy coefficient for the ion- ^1H rotor is approximately 2 corresponding to a Brownian rotational diffuser. For a Brownian rotor,

$$P(\beta, t) = N(t) \left[1 + 2 \sum_{p=1}^{\infty} e^{-p^2 t/\tau} \cos p\beta \right] \quad (\text{A9})$$

where the normalisation term $N(t)$ is given by Eq. (A8) with $\alpha = 2$. Substituting Eq. (A9) into Eq. (A4) and executing the elementary integrals yields

$$G(t) = \frac{16\delta N_M N(t)}{a^4} \sum_{p=2,4,\dots}^{\infty} \frac{e^{-p^2 t/\tau} p^2}{(9-p^2)(p^2-1)}. \quad (\text{A10})$$

Finally, combining Eq. (A10) with Eq. (A8) and expanding the exponentials as a series produces Eq. (7) in the main text.

REFERENCES

- ¹N. Bloembergen, E. M. Purcell, and R. V. Pound, *Phys. Rev.* **73**, 679 (1948).
- ²I. Aime, M. Botta, and E. Terreno, *Advances in Inorganic Chemistry: Relaxometry of Water-Metal Ion Interactions*, edited by I. Bertini and R. van Eldik (Elsevier, San Diego, 2005) pp. 173–237.
- ³D. Pan, A. H. Schmieder, S. A. Wickline, and G. M. Lanza, *Tetrahedron* **67**, 8431 (2011).
- ⁴I. Bertini, C. Luchinat, and G. Parigi, *Advances in Inorganic Chemistry: Relaxometry of Water-Metal Ion Interactions*, edited by I. Bertini and R. van Eldik (Elsevier, San Diego, 2005) pp. 105–172.
- ⁵P. R. Bodart, A. Rachocki, J. Tritt-Goc, B. Michalke, P. Schmitt-Kopplin, T. Karbowiak, and R. D. Gougeon, *Talanta* **209**, 120561 (2020).
- ⁶S. Baroni, R. Consonni, G. Ferrante, and S. Aime, *J. Agric. Food Chem.* **57**, 3028 (2009).
- ⁷J.-P. Korb, *New J. Phys.* **13**, 035016 (2011).
- ⁸I. Solomon, *Phys. Rev.* **99**, 559 (1955).
- ⁹I. Solomon and N. Bloembergen, *J. Chem. Phys.* **25**, 261 (1956).
- ¹⁰G. Laukien and J. Schlüter, *Z. Phys.* **146**, 113 (1956).
- ¹¹L. Morgan and A. Nolle, *J. Chem. Phys.* **31**, 365 (1959).
- ¹²N. Bloembergen and L. Morgan, *J. Chem. Phys.* **34**, 842 (1961).
- ¹³I. Bertini, C. Luchinat, and G. Parigi, *Solution NMR of paramagnetic molecules: applications to metalloproteins and models* (Elsevier, 2001) Chap. 7.
- ¹⁴D. A. Faux, A. A. Rahaman, and P. J. McDonald, *Phys. Rev. Lett.* (2021).
- ¹⁵A. G. Redfield, *Phys. Rev.* **98**, 1787 (1955).
- ¹⁶A. Abragam, *Principles of nuclear magnetism* (Clarendon Press, Oxford, 1961).
- ¹⁷D. A. Faux and P. J. McDonald, *Phys. Rev. E* **95**, 033117 (2017).
- ¹⁸A. Messiah, *Quantum Mechanics* (North Holland Press, 1965).
- ¹⁹C. Sholl, *J. Phys. C: Solid State Physics* **7**, 3378 (1974).
- ²⁰K. R. Brownstein and C. E. Tarr, *Phys. Rev. A* **19**, 2446 (1979).
- ²¹L.-P. Hwang and J. H. Freed, *J. Chem. Phys.* **63**, 4017 (1975).
- ²²K. Krynicky, C. D. Green, and D. W. Sawyer, *Faraday Discuss. Chem. Soc.* **66**, 199 (1978).
- ²³L. Helm, *Prog. Nucl. Magn. Reson. Spectrosc.* **49**, 45 (2006).
- ²⁴J. Kowalewski, L. Nordenskiöld, N. Benetis, and P.-O. Westlund, *Prog. Nucl. Magn.*

- Reson. Spectrosc. **17**, 141 (1985).
- ²⁵L. Helm and A. E. Merbach, Chem. Rev. **105**, 1923 (2005).
- ²⁶H. C. Torrey, Phys. Rev. **92**, 962 (1953).
- ²⁷D. A. Faux, D. K. Ross, and C. A. Sholl, J. Phys. C: Solid State Phys. **19**, 4115 (1986).
- ²⁸H. Friedman, M. Holz, and H. Hertz, J. Chem. Phys. **70**, 3369 (1979).
- ²⁹S. M. Abernathy and R. R. Sharp, J. Chem. Phys. **106**, 9032 (1997).
- ³⁰D. A. Faux, S.-H. P. Cachia, P. J. McDonald, J. S. Bhatt, N. C. Howlett, and S. V. Churakov, Phys. Rev. E **91**, 032311 (2015).
- ³¹S. Plimpton, J. Comput. Phys. **117**, 1 (1995).
- ³²A. Jewett, *Moltemplate manual* (University of California, Santa Barbara Shea Lab, 2020).
- ³³H. Berendsen, J. Postma, W. Van Gunsteren, and J. Hermans, *Interaction models for water in relation to protein hydration* (Springer, 1981) p. 331.
- ³⁴H. J. C. Berendsen, J. R. Grigera, and T. P. Straatsma, J. Phys. Chem. **91**, 6269 (1987).
- ³⁵P. Mark and L. Nilsson, J. Phys. Chem. A **105**, 9954 (2001).
- ³⁶I. S. Joung and T. E. Cheatham III, J. Phys. Chem. B **112**, 9020 (2008).
- ³⁷I. S. Joung and T. E. Cheatham III, J. Phys. Chem. B **113**, 13279 (2009).
- ³⁸S. Nosé, Mol. Phys. **52**, 255 (1984).
- ³⁹C. J. Meledandri and D. F. Brougham, Anal. Methods **4**, 331 (2012).
- ⁴⁰Y. Ducommun, K. E. Newman, and A. E. Merbach, Inorg. Chem. **19**, 3696 (1980).
- ⁴¹T. W. Swaddle and A. E. Merbach, Inorg. Chem. **20**, 4212 (1981).
- ⁴²M. Grant and R. Jordan, Inorg. Chem. **20**, 55 (1981).
- ⁴³D. H. Powell, L. Helm, and A. E. Merbach, J. Chem. Phys. **95**, 9258 (1991).
- ⁴⁴K. Krynicki, Physica **32**, 167 (1966).
- ⁴⁵P. Smirnov and O. Grechin, Russ. J. Phys. Chem. A **93**, 2213 (2019).
- ⁴⁶S. H. Koenig and R. D. Brown III, Magn. Reson. Med. **1**, 478 (1984).
- ⁴⁷G. Hernandez and R. G. Bryant, Bioconj. Chem. **2**, 394 (1991).
- ⁴⁸I. Bertini, F. Capozzi, C. Luchinat, and Z. Xia, J. Phys. Chem. **97**, 1134 (1993).
- ⁴⁹I. Bertini, F. Capozzi, C. Luchinat, G. Nicastro, and Z. Xia, J. Phys. Chem. **97**, 6351 (1993).
- ⁵⁰M. Magini and T. Radnai, J. Chem. Phys. **71**, 4255 (1979).
- ⁵¹R. Hausser and F. Noack, Z. Phys. **182**, 93 (1964).
- ⁵²J. R. Bell, J. L. Tyvoll, and D. L. Wertz, J. Am. Chem. Soc. **95**, 1456 (1973).

⁵³M. Magini, J. Chem. Phys. **74**, 2523 (1981).

⁵⁴D. A. Faux, P. J. McDonald, and N. C. Howlett, Phys. Rev. E **95**, 033116 (2017).